Tides in shallow water: Spectroscopy

By BRENT S. GALLAGHER[1] and WALTER H. MUNK[2], [1]*Department of Oceanography, University of Hawaii, Honolulu, Hawaii 96822,* and [2]*The Institute of Geophysics and Planetary Physics, University of California, San Diego, California 92037, USA*

(Manuscript received March 3, 1971)

ABSTRACT

Non-linear distortions of long waves (tides) in shallow water are analysed. The effects of finite wave amplitude, bottom slope, friction, and multi-chromatic interactions are investigated separately and in combination, using both perturbation analysis and numerical solutions of the full non-linear equations. The distortions caused by each source of non-linear behavior are presented in the time and frequency domains, and some implications of the results for local and ocean-wide tide predictions are discussed.

1. Concerning tide prediction

In the harmonic method, the tidal elevation at a given port is predicted according to

$$\xi(t) = \sum_k C_k \cos(2\pi f_k t + \theta_k) \qquad (1.1)$$

summed over a denumerable set of frequencies f_k. For each of these frequencies, the station constants C_k and θ_k are determined from an analysis of a past tide record. The method is at its best at stations with steep off-shore shelves, such as Honolulu, Hawaii. Here 20 frequencies, requiring 40 station constants, can account for all but 0.1% of the observed tidal variance. This residual (observed minus predicted) tidal variance is so small compared to the atmospheric residual (typically 1% to 10% of the observed variance) as to make any improvement in tide prediction a sterile exercise.

At ports opposite broad shallow shelves and at the upper ends of bays, the tidal residuals may be of the order of 10% even after several hundred frequencies have been taken into account. The new frequencies are produced by the distortion of the incident waves (leading ultimately to a bore formation). The situation may be likened to two non-linear processes in series: (i) the non-linearity associated with Kepler-Newton mechanics generates harmonics of the fundamental frequencies, and furthermore produces a fine-structure with monthly, yearly and nodal splitting. (ii) the non-linearities associated with Navier-Stokes hydrodynamics generate further frequency sums and differences as the tide wave travels across a shallow shelf.

Kepler-Newton splitting produces some strong lines of very nearly the same frequency (e.g., S_2 and K_2 at 2.000 and 2.006 cycles per day, respectively). Resonances in the ocean basin are relatively broad, and the response to these neighboring frequencies must be sensibly the same. Yet by the harmonic method, the tidal constants for these two frequencies are evaluated as if they were independent! Accordingly, Munk & Cartwright (1966) propose to define by a set of constants the *response* of a station to various input functions. The prediction is performed in the time domain by generating suitable tidal input functions, and then "playing" these through the appropriate station filters. There is no need for time-harmonic (only spherical-harmonic) expansion; all the spectral complexity of Kepler-Newton mechanics is already contained in the input functions, and these are readily generated from fundamental principles using the known orbital constants.

But if there is to be any advantage in working in the time domain for steep island stations where the prediction accuracy is already so high, the advantage is much enhanced for shallow water ports. The present study is an inquiry into the non-linear distortions undergone by long waves in shoal water. This is a worthwhile prelude to constructing a non-linear tide prediction method based on the ideas ex-

pressed above, and it is interesting by itself as well. Throughout the inquiry, we repeatedly examine a system in which linear waves from deep water are incident upon a shoal shelf which borders a reflecting shore. To gain understanding, we treat each cause of non-linear behavior separately—to discover the isolated effects of factors such as incident wave amplitude and bottom friction. These effects are approached in both the time and frequency domains, and the results of second-order perturbation theory are compared with complete computer solutions in almost every case. The perturbation solutions give analytic insight into the basic mechanisms present; the computer first serves as a check, and then as a means to explore more strongly non-linear situations where analysis is intractable.

2. The one-dimensional shallow water equations

(a) *Nature of the approximations*

Linear wave theory assumes that

$$\varepsilon_1 = \tilde{\varkappa}\tilde{a}, \quad \varepsilon_2 = \tilde{a}/\tilde{h}$$

are small quantities. Interactions can be studied by taking terms in ε, ε^2, ... into account, but the interactions are of different types, depending on whether ε_1 or ε_2 is the limiting parameter: ε_1-interactions involve "frequency-dispersive waves" with depth as a negligible factor; in the case of diminishing depth the parameter ε_2 ultimately predominates, and this leads to "amplitude-dispersive" waves in shallow water and an analogy with gas dynamics.

In most cases, ε_1 and ε_2 are both small, and it is not immediately clear which interaction (if any) predominates. It was shown by Stokes (Ursell, 1953) that

$$\phi = \frac{\varepsilon_1^2}{\varepsilon_2^3} = \frac{\tilde{\varkappa}^2\tilde{h}^3}{\tilde{a}}$$

is the pertinent ratio, with ε_1-interactions corresponding to $\phi \gg 1$, and ε_2-interactions to $\phi \ll 1$; for ϕ of order 1 it is possible to attain a balance between amplitude and frequency dispersions, leading to the solitary waves of permanent form discovered by Boussinesq.

Typical offshore values for tidal amplitudes, wave length and depth are

$$\tilde{a} = 1 \text{ m}, \quad 2\pi\tilde{\varkappa}^{-1} = 1\,000 \text{ km}, \quad \tilde{h} = 1 \text{ km}$$

and hence $\varepsilon_1 = 10^{-5}$, $\varepsilon_2 = 10^{-3}$, $\phi = 10^{-1}$. In shoaling water $\tilde{\varkappa}^2\tilde{h}$ and $\tilde{a}^4\tilde{h}$ remain roughly constant, so that $\phi \sim \tilde{h}^{9/4}$. At the edge of the continental shelf $\tilde{h} = 100$ m, and so $\phi \approx 10^{-3}$, and further inshore ϕ is even smaller. The conclusion is that the shallow water equations form a suitable starting point.

We avoid two critical situations that can occur within the framework of shallow water theory. If $\tilde{a}$ were to exceed $\tilde{h}$, the bottom would be exposed, corresponding to *cavitation* in the gas-dynamical analogy. Thus the ratio $\varepsilon_2 = \tilde{a}/\tilde{h}$ (henceforth the dimensionless amplitude a) must be less than unity. Secondly, for sufficiently long, shallow channels the tide may break, corresponding to *shock* formation. In nature the occurrence of "tidal bores" is rare, but when they do occur the local curvature (which can be roughly equated to $\tilde{\varkappa}$) may increase to a point where ϕ is large and frequency dispersion important. This situation and the associated possible development of undulatory tidal bores is beyond the scope of this paper.

(b) *The shallow water equations*

A convenient set of dimensionless variables are:

$$x = \frac{\tilde{x}}{\tilde{L}}, \quad t = \frac{\tilde{t}}{\tilde{L}/\tilde{c}}, \quad a = \frac{\tilde{a}}{\tilde{H}}, \quad u = \frac{\tilde{u}}{\tilde{c}}, \quad \tilde{c} = \sqrt{g\tilde{H}}$$

and

$$\omega = \frac{\tilde{\omega}}{\tilde{c}/\tilde{L}}, \quad \varkappa = \tilde{\varkappa}\tilde{L}$$

In this notation $\omega = \varkappa$ for waves travelling at a (dimensional) speed $\tilde{\omega}/\tilde{\varkappa} = c$. The equations are

$$h_t + (uh)_x = 0 \tag{2.1}$$

$$u_t + uu_x + \zeta_x = 0, \quad \zeta = h - H, \tag{2.2}$$

and we use the boundary conditions

$$[\zeta(t) + u(t)] \text{ specified at } x = 0 \tag{2.3}$$

$$u = 0 \quad \text{at } x = 1. \tag{2.4}$$

Condition (2.3) amounts to specifying an incident wave from deep water where non-

linearities are assumed negligible. It turns out that most essential features of the non-linear tide can be discussed in terms of the simplest possible model, $\tilde{H}$ = constant, hence $H = 1$; we shall do so in some detail before going to complex situations.

The boundary condition (2.4) implies a reflecting wall at $\tilde{x} = \tilde{L}$. We visualize the wall just off the coast line at a depth somewhat exceeding the largest tidal amplitude. This avoids "cavitation", and greatly simplifies numerical calculations without significantly altering the essential results. We shall also avoid bore (shock) formation; in an infinitely long channel of constant depth, a bore is first formed (Stoker, 1957, p. 356) where $\tilde{x} = \tilde{x}_b = 2\tilde{c}_0^3/(3g\,\tilde{a}\,\tilde{\omega})$. The condition $\tilde{x}_b > \tilde{L}$ implies $a\omega < 2/3$. In summary, we are limited to the conditions

$$a < 1, \quad a\omega < 2/3 \qquad (2.6\text{a,b})$$

to avoid cavitation and shock, respectively

(c) *Numerical treatment*

The procedure to be adopted is to compare second-order analytical solutions with the (presumably) complete non-linear solutions from computer experiments. Various numerical schemes are available, and after some experimentation, we adopted a Lax-Wendroff scheme which has previously been applied by Keller & Keller (1964) to the propagation of non-dissipative waves over a bottom of constant slope. The Lax-Wendroff method is inherently stable (under a Courant condition) up to and including bore formation, at the expense of some numerical damping and computing efficiency. Also, matter is not precisely conserved. We chose a computational grid sufficiently fine to bring the energy and mass losses within acceptable limits.

We have expanded the Keller & Keller programs to allow treatment of arbitrary channel topographies (breadth and depth), and have added quadratic bottom friction (§4). Although a variety of boundary conditions are present as options in the expanded code, the numerical solutions described here have used a sea wall at the inshore boundary and a specified incident wave entering an initially undisturbed channel. Transients are allowed to die out before the solutions are analysed; usually this occurs after a wave has traversed the channel four times ($t = 4$).

3. Wave steepening

(a) *Approximate solutions*

We ignore friction, and limit the discussion to a shelf of fixed depth. Very near the origin we prescribe the wave system to consist of incident waves of frequency ω and amplitudes[1] a, plus reflected waves of frequencies ω, and 2ω, ..., and of undetermined (complex) amplitudes $\alpha_1, \alpha_2, \ldots$:

$$\zeta_0(t) = \mathrm{Re}\,\{a\,e^{-i\omega(t-x)} + \alpha_1 e^{-i\omega(t+x)} + \alpha_2 e^{-2i\omega(t+x)} + \ldots\} \qquad (3.1)$$

$$u_0(t) = \mathrm{Re}\,\{a\,e^{-i\omega(t-x)} - \alpha_1 e^{-i\omega(t+x)} - \alpha_2 e^{-2i\omega(t+x)} - \ldots\}$$

Solutions are written in the form

$$\zeta(x,t) = \mathrm{Re}\,\{f_0 + f_1 e^{-i\omega t} + f_2 e^{-2i\omega t} + \ldots\}$$
$$u(x,t) = \mathrm{Re}\,\{u_1 e^{-i\omega t} + u_2 e^{-2i\omega t} + \ldots\}, \qquad (3.2)$$

where $f_n(x)$, $u_n(x)$ are undetermined complex functions.

There could be some objection to expressing the wave system at the origin as a superposition of incident and reflected waves; such a separation requires that the waves behave linearly (locally). But if nonlinearity is important in the inshore zone, it might be important at the offshore origin as well, because depth is everywhere the same. We have previously solved the problem for the case of a step bottom topography with linearity specified in the deep water, $x < 0$, and matching conditions on ζ_x and Hu at $x = 0$. The algebra is much more cumbersome, yet with physical results substantially the same as those from the present treatment in which we artificially endow the system with linearity for negative x. All these difficulties disappear in cases where depth increases offshore.

Frequency ω to order a. Substitute solutions (3.2) into the equations (2.1) to (2.4), and expand products of trigonometric terms into sum

[1] The dimensionless variables are so chosen that the amplitudes of displacement ζ and velocity u are the same.

and difference frequencies.[1] Then to first order in the dimensionless amplitudes a, we have

$$\omega f_1 + iu_{1,x} = 0 \quad f_{1,x} - i\omega u_1 = 0 \qquad (3.3a,b)$$

$$a + \alpha_1 = f_1(0) \quad a - \alpha_1 = u_1(0) \qquad (3.3c,d)$$

$$u_1(1) = 0 \qquad (3.3e)$$

with the solutions

$$f_1 = 2a\, e^{i\omega} \cos \omega(x-1), \quad u_1 = 2aie^{i\omega} \sin \omega(x-1)$$

$$\alpha_1 = ae^{2i\omega} \qquad (3.4)$$

To this order the amplitude α_1 of the reflected wave equals the amplitude a of the incident wave.

Frequency 2ω. Collecting terms in $2\omega t$, we have

$$2\omega f_2 + iu_{2,x} = -\tfrac{1}{2}i(f_1 u_1)_x$$
$$= 2a^2\omega e^{2i\omega} \cos 2\omega(x-1)$$

$$f_{2,x} - 2i\omega u_2 = -\tfrac{1}{2}u_1 u_{1,x}$$
$$= a^2\omega e^{2i\omega} \sin 2\omega(x-1)$$

$$\alpha_2 = f_2(0) = -u_2(0), \quad u_2(1) = 0$$

with the solution

$$f_2 = a^2 W \cos 2\omega(x-1) + \tfrac{3}{2}a^2\omega(x-1)e^{2i\omega} \sin$$
$$2\omega(x-1) + \tfrac{1}{4}a^2 e^{2i\omega} \cos 2\omega(x-1) \qquad (3.6)$$

$$u_2 = a^2 iW \sin 2\omega(x-1) - \tfrac{3}{2}a^2 i\omega(x-1)e^{2i\omega}$$
$$\cos 2\omega(x-1)$$

where

$$W = -\tfrac{1}{8}[e^{6i\omega} + (1 + 12i\omega)e^{2i\omega}].$$

The homogenous solution $W e^{2i\omega(x-1)}$ has the same x-dependence as the forcing function, and this gives rise to terms with amplitudes proportional to $x-1$. In the case of no reflecting wall, these terms correspond to the familiar Airy solution (Lamb, 1932 p. 281) having a linear growth with x. The no-shock condition 2.6b assures that the approximation not be carried to the breaking point.

Terms of zero frequency—From equations (2.2) and (2.3) one finds

$$f_{0,x} = -\tfrac{1}{4}(u_1 u_1^*)_x = -a^2\omega \sin 2\omega(x-1)$$

$$f_0(0) = 0$$

so that

$$f_0(x) = \tfrac{1}{2}a^2[\cos 2\omega(x-1) - \cos 2\omega] \qquad (3.7)$$

Frequency ω *to higher order*—Collecting again terms in frequency ω we find

$$\omega f_1 + iu_{1,x} = [-if_0 u_1 - \tfrac{1}{2}if_1^* u_2$$
$$-\tfrac{1}{2}if_2 u_1^*]_x = \text{order } (a^3) \qquad (3.8a)$$

$$f_{1,x} - i\omega u_1 = -\tfrac{1}{2}[u_1^* u_2]_x = \text{order } (a^3) \qquad (3.8b)$$

$$a + \alpha_1 = f_1(0), \quad a - \alpha_1 = u_1(0) \quad u_1(1) = 0 \qquad (3.8c)$$

The terms u_1, f_1 appearing to the left in (3.8a,b) are the linear solutions (3.4). One now obtains

$$f_1 = 2ae^{i\omega} \cos \omega(x-1) + \text{order } (a^3)$$

$$u_1 = 2aie^{i\omega} \sin \omega(x-1) + \text{order } (a^3)$$

$$\alpha_1 = ae^{2i\omega} + \text{order } (a^3)$$

There are also terms of order a^3 at frequency 3ω.

(b) *Numerical examples*

In Table 1, the column $\tilde{k}^2 = 0$ (no friction) gives a comparison between the foregoing solutions and the results of numerical integrations. The example portrays a semidiurnal wave over a broad, shallow shelf. The amplitude is taken very low (5 cm) to afford a check of perturbation theory:

$$\tilde{L} = 750 \text{ km} \quad \tilde{H} = 16 \text{ m}, \quad \tilde{T} = 2\pi/\tilde{\omega} = 12^h.$$

$$\tilde{a} = 5 \text{ cm}, \quad a = 0.00313$$

$$\omega = 8.72\, \tfrac{3}{2}a\omega = 0.041$$

The numerical results were obtained using $\Delta x = 0.005$ and $\Delta t = T/180$. Thus $\tilde{\Delta}x = 3.85$ km, $\tilde{\Delta}t = 0.067$ hours.

Agreement is generally within a few percent. The only notable discrepancy occurs for the mean terms, f_0. But here it is noted that the computer scheme yields a non-zero displacement at the offshore origin, and when this is allowed for (numbers in parentheses) the agreement is much improved. For comparison, we

[1] The products $\mathrm{Re}\{f_m e^{-im\omega t}\}$ $\mathrm{Re}\{f_n e^{-in\omega t}\}$ are implied, and not $\mathrm{Re}\{f_m e^{-im\omega t} \quad f_n e^{-in\omega t}\}$

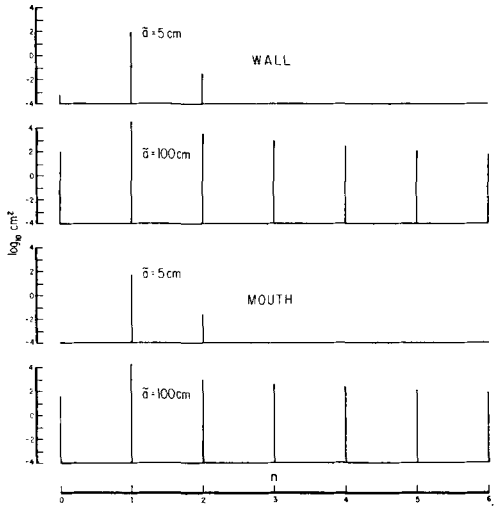

Fig. 1. The "energy" I_n/I_n^* of harmonic n at frequency $n\omega$ associated with an incident sinusoid of amplitude a at frequency ω. The upper two panels correspond to conditions at the inner wall, the lower panels to the mouth of a bay of constant depth, and of length $\omega/2\pi = 1.39$ times the wave length. There is no friction.

have displayed the two cases

$$\tilde{a} = 5 \text{ cm}, \quad \omega = 8.72, \quad a = 0.00313,$$

$$a\omega = 0.027$$

$$\tilde{a} = 100 \text{ cm} \quad \omega = 8.72, \quad a = 0.0625,$$

$$a\omega = 0.545$$

in the upper panels of Fig. 1. The second case corresponds to near-shock conditions at the wall, and accordingly the harmonics are much enhanced. The next two panels show the corresponding results at the mouth. We note the following conclusions:

(i) The amplitude of the n'th harmonic (frequency $n\omega$) relative to that of the incident wave (frequency ω) is of order a^{n-1}.

(ii) The principal energy loss is from back radiation of the second harmonics and proportional to a^4 (third panel). Thus with a^2 and α^2 proportional to incident and reflected ω-energy, respectively, we have

$$a^2 - \alpha^2 = \text{order } (a^4), \text{ so}$$

$$\alpha = a - \text{order } (a^3) + \ldots,$$

as found by perturbation. It will be shown that frictional losses lead to a reduction of amplitudes of order (a^2).

(iii) There is a change in mean sea level of order $\tilde{a}(\tilde{a}/\tilde{H})$. This is in accordance with the concept of radiation stress introduced by Longuet-Higgins & Stewart (1964). Changes in mean sea level of the expected amounts have been reported by Unoki & Isozaki (1965) for some Japanese bays. There is no change of mean level for an open ended channel.

So far the results obtained are simple and expected. But they pave the way for a more realistic situation.

4. Friction

We add a term

$$\text{dimensional:} \quad -\tilde{H}^{-1}\tilde{k}^2\tilde{u}|\tilde{u}|$$

$$\text{dimensionless:} \quad -k^2H^{-1}u|u|, \; k^2 = \tilde{k}^2\tilde{L}/\tilde{H}$$

on the right-hand side of equation (2.2). There is sufficient evidence from a variety of sources to warrant this form of dissipative non-linearity: from boundary layer theory, laboratory measurements and measurements near the sea bottom (Bowden & Fairbairn, 1952), and finally from the observed tidal dissipation in the Irish Sea (Taylor, 1919) and River Thames (Rossiter & Lennon, 1965). "Observed" values of $\tilde{k}^2$ range from 0.001 to 0.003. For shelves the ratio $\tilde{L}/\tilde{H}$ may vary between 10^2 and 10^4. This puts the range of k^2 from 0.1 to 10, indicating that one may expect a variety of conditions ranging from negligible to predominant effects of friction

(a) *Approximate solutions*

Expanding the first order solution, we have

$$\text{Re}(u_1 e^{i\omega t}) = -2a \sin\xi \sin\omega(t-1)$$

$$|u| = \frac{8a|\sin\xi|}{3\pi} \times [\tfrac{1}{2} - \tfrac{1}{3}\cos 2\omega(t-1) - \tfrac{1}{15}\cos 4\omega(t-1) + \ldots]$$

$$u|u| = -\frac{32a^2 \sin^2\xi\, s(\xi)}{3\pi} \times [\sin\omega(t-1) - \tfrac{1}{5}\sin 3\omega(t-1) + \ldots] \qquad (4.1)$$

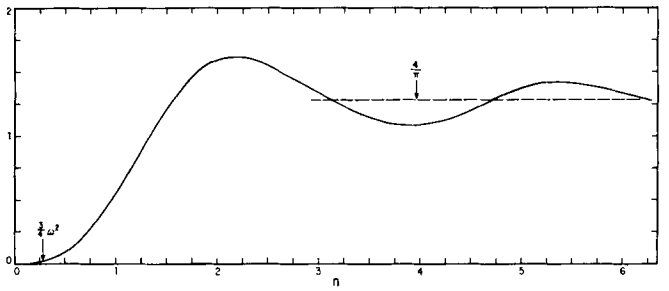

Fig. 2. The function $\phi_1(\omega)$ giving the frictional reduction of reflected ω-amplitude as function of frequency.

where $\xi = -\omega(x-1)$, and $s(\xi) = \pm 1$ according to whether $\sin\xi$ is positive or negative. The terms are of order a^2 and converge slowly with increasing frequency. But we note that the zero-crossings of $[\sin\omega(t-1) - \frac{1}{3}\sin 3\omega(t-1) + \ldots]$ occur for the same times as the zero-crossings of $\sin\omega(t-1)$, so that the expression for $u|u|$ has *precisely* the sign of u; away from the zero-crossings, at $\omega(t-1) = \frac{1}{2}\pi$, say, the precise magnitude of u^2 is $4a^2\sin^2\xi$, as compared to $(\frac{32}{3}\pi)a^2\sin^2\xi[1 + (\frac{1}{3}) - \ldots] = (3.40 + 0.68 - \ldots)a^2 \sin^2\xi$ for the approximate expression.

Frequency ω. Equations (3.3c, d, e) are unchanged. Equations (3.3a, b) are written (omitting subscripts 1)

$$f - iu_\xi = 0 \qquad -f_\xi - iu = +3iKe^{i\omega}\sin^2\xi\, s(\xi), \tag{4.2a, b}$$

where

$$K = \frac{32}{9\pi}k^2a^2\omega^{-1}$$

The equations can be combined into

$$u_{\xi\xi} + u = -3Ke^{i\omega}s(\xi)\sin^2\xi = F(\xi), \text{ say,}$$

and this has the general solution

$$u(\xi) = \int_0^\xi F(\xi')\sin(\xi-\xi')\,d\xi' + A\sin\xi$$

$$f(\xi) = +iu_\xi = i\int_0^\xi F(\xi')\cos(\xi-\xi')\,d\xi' + iA\cos\xi$$

which obeys the boundary condition $u(0) = 0$. The integrals yield

$$u_1(\xi) = -Ke^{i\omega}[-4n\cos\xi + 2(1 - s\cos\xi)^2] + A_1\sin\xi$$

$$f_1(\xi) = -iKe^{i\omega}[4n\sin\xi + 2(1 - s\cos\xi)\sin\xi] + iA_1\cos\xi \tag{4.3}$$

where $s = s(\xi)$, and n is defined by $\xi = n\pi + \Delta$, with $\Delta \leqslant 180°$. $n(\xi)$ is the number of nodes between any point x and the wall. It follows that

$$s = +1 \text{ for even } n, \quad s = -1 \text{ for odd } n.$$

To determine A, we use the complex patching conditions

$$a + \alpha_1 = f_1(0), \quad a - \alpha_1 = u_1(0).$$

$u_1(1) = 0$ at $x = 0$, so at $\xi = \omega$, $s = s(\omega)$; $n(\omega)$ is now the total number of nodes in the channel. The result is

$$iA_1 = e^{i\omega}\{2a - K[\tfrac{1}{4}s\,e^{3i\omega} - \tfrac{3}{2}s\,e^{i\omega} + 4n + 2 - \tfrac{3}{4}s\,e^{-i\omega}]\}$$

It is convenient to write $f_1(\xi) = f_1^{(1)} + f_2^{(2)} + \ldots$ where $f_1^{(1)}$ is the solution (3.4) of order a, and

$$f_1^{(2)} = -\frac{32}{9\pi}k^2a^2\omega^{-1}e^{i\omega}\{[4n(\xi) + 2 - 2s(\xi)\cos\xi]\,i\sin\xi + [\tfrac{1}{4}s(\omega)e^{3i\omega} - \tfrac{3}{2}s(\omega)e^{i\omega} + 4n(\omega) + 2 - \tfrac{3}{4}s(\omega)e^{-i\omega}]\cos\xi\}$$

is the frictional contribution of order a^2 at frequency ω. The reflected amplitude at $x = 0$ ($\xi = \omega$) is given by

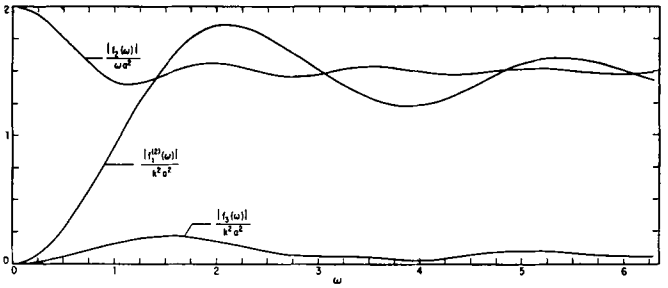

Fig. 3. Modulus of the non-linear amplitude func- tions at the sea wall, $x = 1$. $f_1(\omega)$ and $f_3(\omega)$ are the results of quadratic friction, $f_2(\omega)$ is due to nonfrictional non-linearities.

$$\alpha_1 = -a + f_1(x=0) = -a + 2a e^{i\omega}\cos\omega + f_1^{(2)}(\omega)$$

$$= a e^{2i\omega} + f_1^{(2)}(\omega) = e^{2i\omega}\left\{a - \frac{32}{9\pi}k^2a^2\phi_1(\omega)\right\} \qquad (4.4)$$

(say), where

$$\omega\phi_1(\omega) = 4n(\omega) + 2 + s(\omega)$$

$$\times(\cos^3\omega - 3\cos\omega = \tfrac{3}{4}\omega^3 + \ldots$$

is always positive (see Fig. 2). Thus, the reflected amplitude equals the incident amplitude, $\alpha = a$, for vanishing friction k^2, and is otherwise always less than a by an amount proportional to k^2a^2.

Frequency 3ω. The equations (omitting subscript 3)

$$3f - iu_\xi = 0, \quad -f_\xi - 3iu =$$

$$-(3/5)iKe^{3i\omega}\sin^2\xi\, s(\xi)$$

can be combined into

$$u_{\xi\xi} + 9u = (9/5)Ke^{3i\omega}\sin^2\xi\, s(\xi) = G(\xi), \text{ say}$$

with the general solution

$$u(\xi) = \int_0^\xi G(\xi')\sin 3(\xi - \xi')d\xi' + A_3\sin 3\xi$$

We find

$$u_3(\xi) = (9/5)Ke^{3i\omega}(1/90)[(8n(\xi) + 4)\cos 3\xi + s(\xi)(5 - 9\cos 2\xi)] + A_3\sin 3\xi \qquad (4.5)$$

$$f_3(\xi) = (9/5)iKe^{3i\omega}(1/90)[-(8n(\xi) + 4)\sin 3\xi + 6s(\xi)\sin 2\xi] + iA_3\cos 3\xi$$

where

$$iA_3 = -\tfrac{1}{100}Ke^{3i\omega}\{16n(\omega) + 8 + s(\omega)[-3e^{5i\omega} + 10e^{3i\omega} - 15e^{i\omega}]\}$$

The non-linear amplitude functions are plotted in Fig. 3.

A comparison of the first two panels of Figs. 1 and 4 shows very clearly the frictional generation of odd harmonics, particularly for high amplitudes.

(b) *Sloping shelf*

For comparison, we have computed the non-linear effects over a beach of constant slope. The parameters are:

	$\tilde{L}$	$\tilde{H}(0)$	$\tilde{H}(\tilde{L})$	$\tilde{T}$
(i) constant depth:	750 km	16 m	16 m	12^h
(ii) constant slope:	750 km	36 m	4 m	12^h

The depths have the relation that the mean root

$$<\tilde{H}^{\frac{1}{2}}> = \tfrac{1}{2}[\sqrt{16} + \sqrt{16}] = \tfrac{1}{2}[\sqrt{36} + \sqrt{4}] = 16 \text{ meters}$$

is the same for (i) and (ii), so that the linear travel time

$$\int_0^{\tilde{L}}\frac{d\tilde{x}}{\tilde{c}} = \frac{\tilde{L}}{\tilde{H}_L - \tilde{H}_0}\int_{\tilde{H}_0}^{\tilde{H}_L}\frac{d\tilde{H}}{\sqrt{(g\tilde{H})}}$$

$$= \frac{\tilde{L}}{\sqrt{g}\,\frac{1}{2}[\tilde{H}_0^{\frac{1}{2}} + \tilde{H}_L^{\frac{1}{2}}]} = \frac{\tilde{L}}{<(g\tilde{H})^{\frac{1}{2}}>} = 16.7^h$$

is the same also. We note from Fig. 4 that the constant depth and constant slope produce similar non-linear effects, and we conclude that

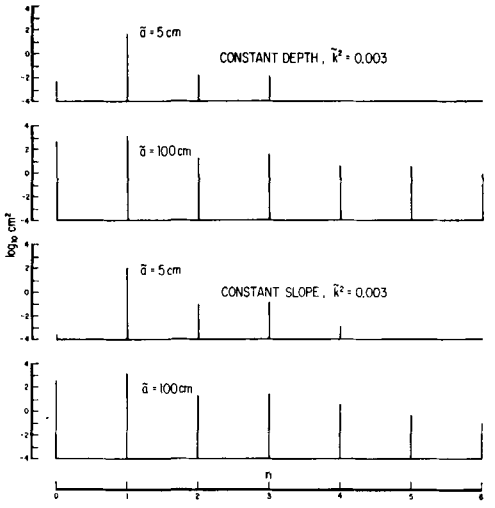

Fig. 4. The effect of friction ($\tilde{k}^2 = 0.003$). The upper panels correspond to conditions at the inner wall of a bay with constant depth, as in Fig. 1. The lower panels refer to equivalent conditions, but with constant bottom slope.

case of variable depth can be usefully discussed[1] in terms of a model whose constant depth is the appropriate square-mean-root (s-m-r, not r-m-s).

(c) *Numerical illustration*

Table 1 compares the approximate analytic solutions with the results of numerical integration. To the present order, friction should affect only odd harmonics. In fact the agreement between numerical and theoretical f_1 and f_3 is satisfactory for $\tilde{k}^2 = 0.001$, but less so for $\tilde{k}^2 = 0.003$. The even harmonics, f_0 and f_2, are not affected in the perturbation theory, but the computed values show a considerable dependence on friction. This is not surprising. The even harmonics depend on products of the quantities f_1, v_1, and in the perturbation analysis only the first order values in a have been used. The actual effect of friction is to alter the quantities f_1 and v_1 through higher order interactions, and the harmonics f_0 and f_2 must be affected accordingly.

We can now reach the following conclusions:

(i) u^2-friction in the perturbation analysis excites principally the odd harmonics, and these are of order a relative to the incident wave. However, sharp reductions of higher harmonics occur in the more complete numerical

[1] There is no inherent difficulty in finding analytic solutions to the case of constant slope, with the Hankel function $H_0(\omega x)^{\frac{1}{2}} = J_0(\omega x)^{\frac{1}{2}} + i\, Y_0(\omega x)^{\frac{1}{2}}$ playing the role of $e^{i\omega x}$.

Table 1. *Comparison between numerical and analytical solutions for stated values of the friction parameter and for* $\omega = 8.72$, $a = 0.00313$

	$\tilde{k}^2 = 0.000$		$\tilde{k}^2 = 0.001$, $k^2 = 47$		$\tilde{k}^2 = 0.003$, $k^2 = 141$	
	Numerical*	Analytical	Numerical*	Analytical	Numerical	Analytical
f_0/a						
$\tilde{x} = 0$	0.00102 (0)	0	0.0060 (0)	0		
$\tilde{x} = \frac{1}{2}\tilde{L}$	−0.00050 (−0.00152)	−0.00143	0.0009 (−0.0051)	0.00143		
$\tilde{x} = \tilde{L}$	0.00225 (0.00123)	0.00131	0.0029 (−0.0031)	0.00131	0.0057	0.00131
f_1/a at $\tilde{x} = \tilde{L}$						
real	−1.495	−1.524	−1.359	−1.356	−1.179	−1.020
imag.	1.273	1.296	1.151	1.146	0.984	0.846
mod.	1.964	2.000	1.781	1.775	1.536	1.325
f_2/a at $\tilde{x} = \tilde{L}$						
real	−0.0389	−0.0380	−0.0328	−0.0380	−0.0249	−0.0380
imag.	−0.0071	−0.0070	−0.0066	−0.0070	−0.0062	−0.0070
mod.	0.0396	−0.0381	0.0334	−0.0381	0.0256	−0.0381
f_3/a at $\tilde{x} = \tilde{L}$						
real	−0.0007		−0.0055	−0.0054	−0.0149	−0.0161
imag.	−0.0010		−0.0080	−0.0091	−0.0200	−0.0273

[a] Numbers in parentheses are corrected for a non-zero displacement at the offshore origin, presumably associated with an apparent mass loss inherent in the Lax-Wendroff computational scheme.

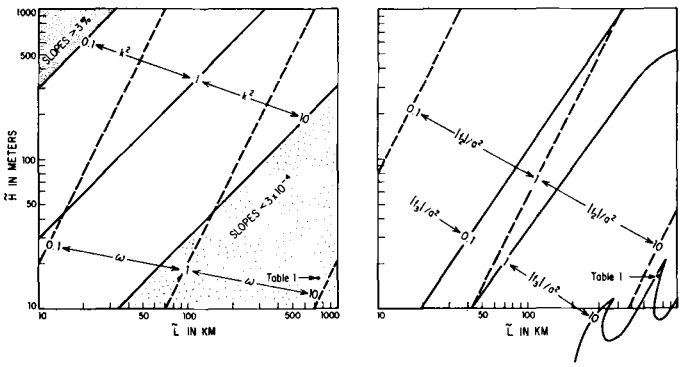

Fig. 5. Left: Lines of equal $k^2 = \tilde{k}^2(\tilde{L}/\tilde{H})$ and $\omega = \tilde{\omega}\,\tilde{L}/\sqrt{g\tilde{H}}$ for $\tilde{k}^2 = 0.003$ and $\tilde{\omega} = 2\pi/12^{\mathrm{h}}$. *Right:* Lines of equal $|f_2|/a^2$ and $|f_3|/a^2$, giving non-linear contributions to the second and third harmonics respectively. The point $\tilde{L} = 750$ km, $\tilde{H} = 16$ m corresponds to the numerical example in Table 1.

treatment. For the case $\tilde{k}^2 = 0.003$ we have the following amplitudes $\tilde{H}|f_n|$ at $\tilde{x} = \tilde{L}$:

harmonic	0	1	2
$\tilde{a} =$ 5 cm,	0.069	7.55	0.126
$\tilde{a} =$ 100 cm,	20.4	39.5	4.3

harmonic	3	4	5
$\tilde{a} =$ 5 cm,	0.115	0.0075	0.0001 cm
$\tilde{a} =$ 100 cm,	6.2	1.99	1.79 cm

(ii) Consider the contributions to the first three harmonics arising from frictional and non-frictional non-linearities, respectively:

	$x = 0$			
	$\omega \ll 1$	$\omega = 1$	$\omega \gg 1$	
$\dfrac{\lvert f_1^{(2)}\rvert}{a^2}$	$0.9\,\omega^3 k^2$	$0.6\,k^2$	$1.45\,k^2$	(frictional)
$\dfrac{\lvert f_2\rvert}{a^2}$	2ω	1.4	$1.5\,\omega$	(non-frictional)
$\dfrac{\lvert f_3\rvert}{a^2}$	$0.50\,\omega^3 k^2$	$0.12\,k^2$	$0.06\,k^2$	(frictional)

	$x = 1$			
	$\omega \ll 1$	$\omega = 1$	$\omega \gg 1$	
$\dfrac{\lvert f_1^{(2)}\rvert}{a^2}$	$1.1\,\omega^2 k^2$	$0.9\,k^2$	$1.45\,k^2$	(frictional)
$\dfrac{\lvert f_2\rvert}{a^2}$	2ω	1.42	1.5ω	(non-frictional)
$\dfrac{\lvert f_3\rvert}{a^2}$	$0.22\,\omega^2 k^2$	$0.16\,k^2$	$0.06\,k^2$	(frictional)

For small $\tilde{\omega} = \tilde{\omega}\,\tilde{L}/\tilde{c}$, e.g. in short and deep basins, all non-linear effects are small. Frictional distortion is *relatively* unimportant for both small and large ω. Near $\omega = 1$, the frictional contribution as evidenced by the ratio f_3/f_2 of the amplitudes of third to second harmonics is of order $0.1k^2 = 0.1\tilde{k}^2(\tilde{L}/\tilde{H})$. The top left curves of Fig. 5 correspond to deep, short basins (or alternately to steep basins with large "square-mean-root depth"); the right bottom corner to shallow or flat shelves. The third harmonic predominates near $\tilde{H} = 10$ meters, $\tilde{L} = 500$ km, but such very shallow, wide basins do not occur in nature and the results of our calculation as shown in Fig. 4 are extreme.

(iii) In accordance with (4.3),

$$|\alpha_1| = \text{a} - \text{order } (\text{a}^2)$$

as compared to a reduction of order (a^3) of reflected relative to incident amplitude for the non-frictional case.

(d) *Tidal dissipation*

Incident and reflected energy flux at the mouth of the basin equal

$$\tfrac{1}{2}\varrho g\tilde{c}(\tilde{a}^2, |\tilde{\alpha}_n|^2) = \tfrac{1}{2}\varrho g\tilde{c}\tilde{H}^2(a^2, |\alpha_n|^2) \qquad (4.6)$$

respectively. Neglecting now all higher harmonics and using (4.4), the energy dissipated (per unit width of basin) is given by

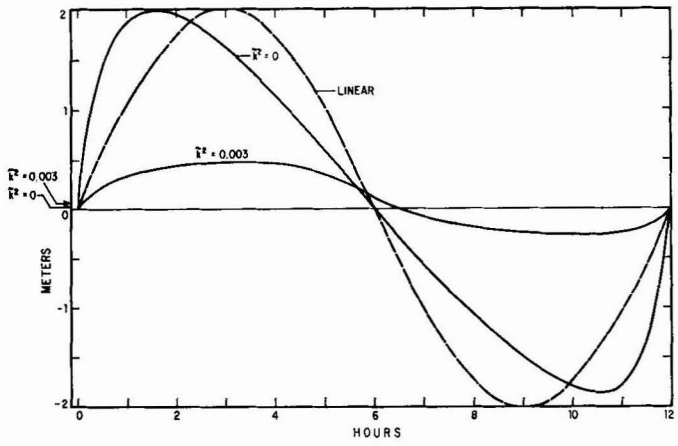

Fig. 6. A tidal cycle at the inner wall of a 750 km channel, 16 m deep, for an incident amplitude of 1 m, period 12^h. The curves show the linear solution, and the results of a computer experiment with and without quadratic friction. Mean sea levels are indicated on the left scale.

$$\tfrac{1}{2}\varrho g\tilde{c}\tilde{H}^2(a^2 - |\alpha_1|^2) = \tfrac{1}{2}\varrho gcH^2 \frac{64}{9\pi} k^2 a^3 \phi_1(\omega)$$

$$= \frac{32}{9\pi}\varrho g^{\frac{1}{2}}\tilde{k}^2\tilde{a}^3\tilde{H}^{-\frac{1}{2}}\tilde{L}\phi_1(\omega) \qquad (4.7)$$

The dissipation can be computed independently as follows. The dissipation per unit area is given by

$$\tilde{k}^2\varrho|\tilde{u}^3| = \tilde{k}^2\varrho\tilde{c}^3|u^3|.$$

Using (3.4) in (3.2) we have to first order $u = -2a \sin\xi \sin\omega(t-1)$, and the time average of $|u^3|$ is then $8a^3\ |\sin^3\xi| < \sin^3\omega(t-1) > = 8a^3|\sin^3\xi|\,(\frac{4}{3}\pi)$.
For the entire basin, the dissipation is given by

$$\tilde{k}^2\varrho\tilde{c}^3\tilde{L}\int_0^1 |u^3|\,dx = \frac{32}{3\pi}\varrho\tilde{k}^2\tilde{c}^3 La^3\omega^{-1}$$

$$\times \int_0^\omega s(\xi)\sin^3(\xi)\,d\xi$$

and this leads *precisely* to the previous result. The result is approximate insofar as we have not allowed for higher order distortion of the wave profile. But we have *not* neglected higher harmonics in $|u^3|$. The agreement with the previous result based only on frequency ω is noteworthy.

Energy dissipation and the generation of the third harmonic are closely related processes. Perhaps the dissipation can be estimated from the amplitude of the third harmonic. For example, taking the expression (4.5) for f_3 at $x = 0$, the energy dissipation is given by

$$\tfrac{1}{2}\varrho g\tilde{c}\tilde{H}^2 a|\alpha_3| \cdot 2e^{4i\omega}|f_1^{(2)}(\omega)|/|f_3(\omega)|.$$

A similar relation can be found for the sea wall.

5. Analysis of extremae

So far the role of non-linearities has been interpreted in terms of the generation of harmonics. This helps establish a link with the harmonic prediction method, and with the substantial body of empirical evidence that has been tabulated in terms of "shallow water constituents." It is closer to the spirit of this paper, and to the goal of prediction, to interpret non-linearities in terms of their effect on the time history.

Fig. 6 shows the distorted wave form for the rather extreme geometry we have used for illustration throughout this paper. The linear solution gives twice the incident wave amplitudes at the wall, 2 m in 16 m of water. We note the following: (i) for the frictionless case the crests are greatly advanced, and the troughs similarly retarded. Friction retards both, and under the present extreme conditions cancels the crest advance. (ii) the heights of crest and trough, when referred to the local mean level, are both very slightly reduced in

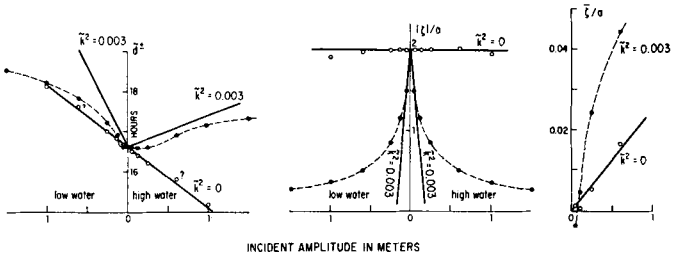

Fig. 7. Retardation (*left*) and amplification (*center*) of high and low water, and mean water level (*right*) computed at the shore for various incident wave amplitudes. Points and connecting dashed curves are from computer experiments, solid curves from second order theory. Geometry as in Fig. 6. Mean levels are relative to the level at the outer boundary. There is some uncertainty concerning the run with $a = 0.6$ m.

the case of no friction, and substantially reduced by friction. (iii) mean water levels are raised 5 cm and 10 cm, respectively[1]. On the basis of a series of computer experiments, the dependence of the delay, amplification and "rectification" on incident amplitudes is plotted in Fig. 7. For the smaller amplitudes we should expect to account for these relations in terms of the perturbation theory.

Times of high and low water are determined by

$$\zeta_t = 0 = \mathrm{Re}\,\{ -i\omega f_1 e^{-i\omega t} - 2i\omega f_2 e^{-2i\omega t} - 3i\omega f_3 e^{-3i\omega t} - \ldots . \} \qquad (5.1)$$

where $f_n(\omega)$ are the functions previously derived. The linear component

$$\mathrm{Re}\,\{ -i\omega f_1^{(1)} e^{-i\omega t} \} = 2a\omega \cos\omega(x-1) \times \mathrm{Re}\,\{ -i\, e^{-i\omega(t-1)} \} \qquad (5.2)$$

vanishes for $t = 1,\ 1 + \pi/\omega \ldots$. The incident crest and trough at $x = 0$ occur at $t = 0,\ \pi/\omega$, respectively. Let $\tau < 1$ be the non-linear retardation, so that

$$t^+ = 1 + \tau^+ = d^+, \quad t^- = \pi/\omega + 1 + \tau^- = \pi/\omega + d^-$$

are the times of high and low water, respectively, and $d^{\pm}$ the associated (linear + nonlinear) delays. Equation (5.2) reduces to $\mp 2a\omega^2 \cos\omega(x-1)\ \tau^{\pm}$ + order (τ^3). τ is of order a, and we can set $t = 1$ and $t = 1 + \pi/\omega$ in the remaining exponentials of equation (5.1). The result is

$$\tau^{\pm} = -\tfrac{1}{2}\omega^{-1}a^{-1}\mathrm{Re}\,\{ +i\, e^{-i\omega} f_1^{(2)} \pm 2i\, e^{-2i\omega} f_2 + 3i\, e^{-3i\omega} f_3 \pm \ldots \} \qquad (5.3)$$
$$= k^2 a\, g_1(\omega) \pm a\, g_2(\omega) + k^2 a\, g_2(\omega), \text{ say.}$$

The functions are plotted in Fig. 8.

Note that τ^+ and τ^- have the same sign if frictionally controlled (g_1, g_3), but opposite sign if controlled by the other non-linearities (g_2). At the wall g_2 approaches $-3/2$ for large ω, hence $\tau^{\pm} \approx \mp(3/2)a$, so that the crests are advanced and the troughs delayed by an amount (in radians)

$$\tilde{\omega}\,|\tilde{\tau}| = \omega\,|\tau| = \tfrac{3}{2}a\omega$$

The shock condition for an infinitely long, non-reflecting channel is $a\omega = 2/3$, and so would correspond to a crest advance (trough delay) by one radian, and a "catching-up" of a crest with respect to the preceding trough by two radians. Breaking requires π radians. Of course this is far beyor d the present approximation, but it is encouraging that the low order theory leads to such sensible results. At $x = 1$ we find $g_1 + g_3$ to be always positive, and we suspect this applies to $g_1 + g_3 + g_5 + \ldots$. Then friction always retards crests and troughs, and by equal amounts (to this order). For the rather extreme case shown in Fig. 7 we have $k^2 = 141$, so that the frictional effects are pronounced even though $g_1 + g_3 < g_2$. The convergence from g_1 to g_2 is poor, and this may account for the poor fit to the frictional delays, even at small amplitudes.

Elevations of crest and trough relative to the mean level at the outer boundary are given by

$$\zeta^{\pm} = \pm 2a \cos\omega(x-1) + \mathrm{Re}\,\{ f_0 \pm f_1^{(2)} e^{-i\omega} + f_2 e^{-2i\omega} \pm f_3 e^{-3i\omega} + \ldots \} \qquad (5.4)$$

[1] Only about half these amounts if allowance is made for a change in mean sea level at the outer boundary. See footnote to Table 1.

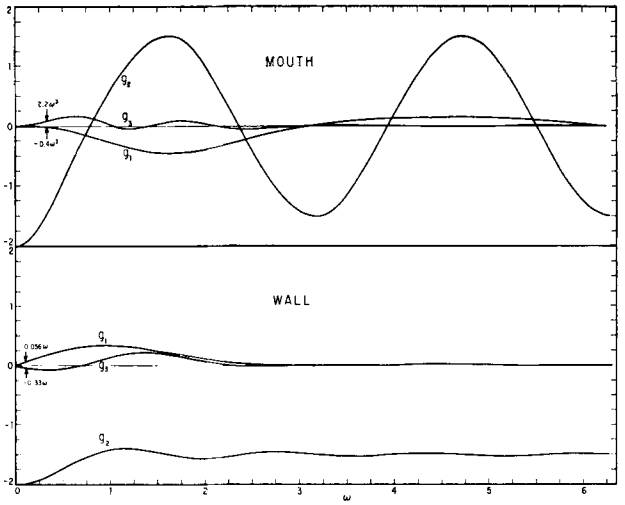

Fig. 8. The "delay" functions $g_n(\omega)$ of equation (5.3) at the outer boundary and sea wall. Asymptotic solutions for small ω are indicated.

(see Fig. 9). f_0 is the displacement in the mean water level; f_2 refers to a wave distortion giving rise to a displacement of high and low water relative to the mean. Since f_0 and f_2 are of the same sign for $\zeta^{\pm}$, they displace crests and troughs by equal amounts without changing the tidal *range*. The frictional terms are of opposite sign for $\zeta^{\pm}$, and so they change the tidal range without displacing the mean level.

At the outer boundary, the f_2-term predominates, and can become large for large ω. The frictional terms are small, and they may increase or decrease the amplitude, depending on ω. At the sea wall, the frictional terms dominate and their sum is always negative, thus leading to a reduction in tidal range. The nonfrictional terms are always positive: the mean level f_0 is always above the mean level at the mouth, and the distortion $\{f_2 e^{-2i\omega}\}$ raises crests *and* troughs even further.

Referring to Fig. 5, we may inquire as to the configurations which favor frictional or non-

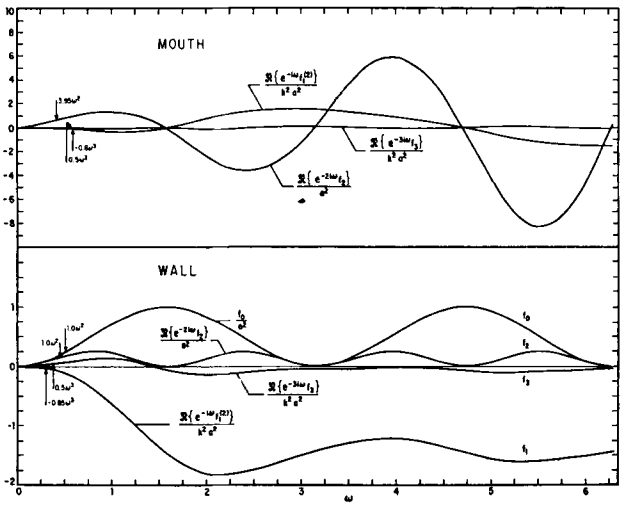

Fig. 9. The "amplification" functions of equation (5.4) at the outer boundary and sea wall. Asymptotic solutions for small ω are indicated.

frictional effects. The appropriate asymptotic relations are:

	$x=0$		
	$\omega \ll 1$	$\omega = 1$	$\omega \gg 1$
Delay functions			
$k^2 g_1$	$-0.4\,\omega^3 k^2$	$-0.25\,k^2$	$\pm 0(\omega^{-1}k^2)$
g_2	-2	$+0.58$	$\pm 0(1)$
Amplification			
$\dfrac{\mathrm{Re}\{e^{-i\omega}f_1^{(2)}\}}{a^2}$	$-0.8\,\omega^3 k^2$	$-0.33\,k^2$	$\pm 0(k^2)$
$\dfrac{\mathrm{Re}\{e^{-2i\omega}f_2\}}{a^2}$	$4.0\,\omega^2$	1.28	$\pm 0(\omega)$

	$x=1$		
	$\omega \ll 1$	$\omega = 1$	$\omega \gg 1$
Delay functions			
$k^2 g_1$	$0.06\,\omega k^2$	$-0.34\,k^2$	$-0(\omega^{-2}k^2)$
g_2	-2	-1.40	-1.50
Amplification			
$\dfrac{\mathrm{Re}\{e^{-i\omega}f_1^{(2)}\}}{a^2}$	$-0.8\,\omega^3 k^2$	$-0.61\,k^2$	$-1.50k^2$
$\dfrac{\mathrm{Re}\{e^{-2i\omega}f_2\}}{a^2}$	$1.0\,\omega^2$	± 0.21	$+0(0.25)$

Various problems can be analysed in terms of $\tilde{L}$, $\tilde{H}$-diagrams (Fig. 5). For example, bore formation calls for $a\omega$ = order (1), hence $\omega \gg 1$. The relative frictional effect at the wall is of order $k^2/\omega^2 = \tilde{k}^2\, g\, \tilde{\omega}^{-2}\, \tilde{L}^{-1}$, which equals unity for $\tilde{k}^2 = 0.003$, $g = 10^3$ cm sec^{-2}, $\tilde{\omega} = 2\pi/12^{\mathrm{h}}$, and $\tilde{L} = 1\,500$ km. It is difficult to find circumstances for which the tendency for radical steepening is not offset by frictional flattening.

6. Multi-chromatic inputs

The discussion so far has been concerned with non-linear distortions of an incident wave of frequency ω. The effect consists of a flux of energy into harmonics $n\omega$ (including $n=0$). Frictional effects favor odd harmonics. The resulting spectra (Figs. 1 and 4) resemble in a qualitative way what is observed at shallow-water ports.

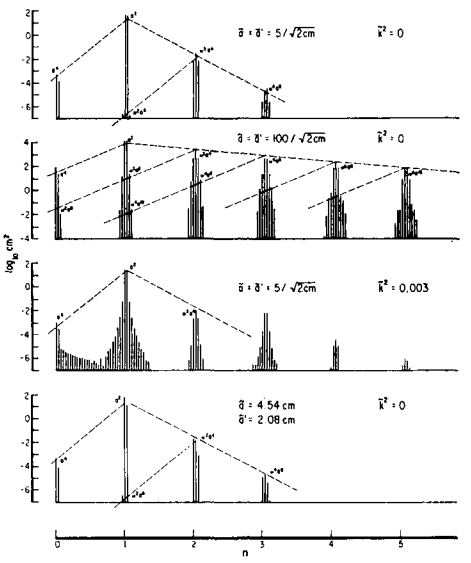

Fig. 10. The spectrum for an incident doublet. In the top two panels the incident doublet carries the same energy as the corresponding singlets in the top two panels of Fig. 1. In the same sense the third panel corresponds to the top panel of Fig. 4. In the bottom panel the doublet is asymmetrical in the ratio of the observed lunar and solar semi-diurnal tides, but carries the same energy. The dashed curves give an approximate measure of side band energy.

There is one observed feature which is beyond the scope of the monochromatic treatment: the input spectrum consists of a narrow cluster of lines near ω, and the observed spectrum at shallow ports shows a further spread of the cluster. Some of the spreading may be the result of non-linear interaction of the line spectrum with the low-frequency continuum, leading to a smudging of each of the lines into a cusp-like continuum (Munk & Cartwright, 1966). Here we are concerned with line-line interactions, leading to multiplet harmonics.

(a) *Incident doublet*

We consider the case of an incident doublet (ω', ω'') arising from the interference between $\omega' = 2$ cycles per lunar day and $\omega'' = 2$ cycles per solar day. The results in Fig. 10 correspond to cases previously analysed, but with the incident "singlet" of frequency ω and amplitude

a replaced by the doublet (ω', ω'') of amplitudes a', a'' such that the singlet energy equals the total incident doublet energy, $a^2 = a'^2 + a''^2$. The multiplet formation is evident, particularly for large amplitudes and friction.

To obtain some analytical insight, we consider the incident doublet

$$\zeta(t) = a' \cos \omega' t + a'' \cos \omega'' t = A \cos(\omega' t + \theta)$$

with

$$A^2(t) = a'^2 + a''^2 + 2a'a'' \cos \sigma t, \quad \tan \theta(t) = \frac{\varrho \sin \sigma t}{1 + \varrho \cos \sigma t}$$

designating the variable amplitude and phase of the interference pattern. Here

$$\varrho = a''/a', \quad \sigma = \omega'' - \omega'.$$

The time origin is spring tide. For $\varrho = 1$,

$$A = 2a' \cos \tfrac{1}{2}\sigma t, \quad \omega' t + \theta = \tfrac{1}{2}(\omega' + \omega'')t.$$

Now set the symmetrical doublet $a' = a'' = \frac{1}{2}\sqrt{2}a$, $\omega' = 29\sigma$, $\omega' = 30\sigma$, with $\sigma = \omega'' - \omega'$ the (dimensionless) difference frequency, 2π radians per fortnight. Thus

$$\tfrac{1}{2}\sqrt{2}a[\cos \omega' t + \cos \omega'' t] = \sqrt{2}a \cos \tfrac{1}{2}\sigma t \cos 29.5\sigma t$$

We can apply all previous solutions by setting

$$\omega \to \tfrac{1}{2}(\omega' + \omega'') = 29.5\sigma, \quad a \to A(t) = \sqrt{2}a \cos \tfrac{1}{2}\sigma t,$$

provided the amplitude varies slowly compared to the time constant of the bay and to the tidal period: $\sigma \ll 1$ and $\sigma \ll \omega$. The essential terms become

		Equivalent multiplet:	
Frequency	Slnglet	amplitudes	energies
"zero"	a^2	$\to a^2[1 + \cos \sigma t]$	$a^4(1 + \frac{1}{2}) = \frac{3}{2}a^4$
$\sim\omega$	$a \cos \omega t$	$\to \frac{\sqrt{2}}{2} a[\cos 29\sigma t + \cos 30\sigma t]$	$\frac{1}{2}a^2(1 + 1) = a^2$
$\sim 2\omega$	$a^2 \cos 2\omega t$	$\to \frac{1}{2}a^2[\cos 58\sigma t + 2 \cos 59\sigma t + \cos 60\sigma t]$	$\frac{1}{4}a^4(1 + 4 + 1) = \frac{3}{2}a^4$
$\sim 3\omega$	$a^3 \cos 3\omega t$	$\to \frac{\sqrt{2}}{4} a^3 [\cos 87\sigma t + 3 \cos 88\sigma t + 3 \cos 89\sigma t + \cos 90\sigma t]$	$\frac{1}{8}a^6(1 + 9 + 9 + 1) = \frac{5}{2}a^6$

The primary frequency is split into a doublet whose combined energy equals (by assumption) the singlet energy. But for 2ω, the multiplet energy is $3/2\ a^4$ as compared to a^4, and for 3ω the energy ratio is 5/2. Thus, incident multiplets generate harmonics with greater energy than do the equivalent singlets. The reason is as follows: the generation of harmonics is larger at spring tides, and less at neap tides, than in the unmodulated case. The departure varies with amplitude, and the positive departure exceeds the negative departure. Within each multiplet the amplitudes have a binominal distribution, and the energies a square-binominal distribution.

Perturbation		*Computer*	
Frequency	Square-binominal	$\tilde{a} = 5$ cm	$\tilde{a} = 1$ m
$\sim\omega$	1 : 1	1 : 1	1 : 1
$\sim 2\omega$	$\frac{1}{4} : 1 : \frac{1}{4}$	0.24 : 1 : 0.24	0.2 : 1 : 0.2
$\sim 3\omega$	$\frac{1}{9} : 1 : 1 : \frac{1}{9}$	0.10 : 0.96 : 1 : 0.11	0.05 : 1 : 1 : 0.05

Instead of the expected doublet: singlet amplifications of 1, 1.5, 2.5 for ω, 2ω and 3ω energies, the computer experiments gave 0.91, 1.17, 1.57 for $a = 5$ cm, and even less for $a = 1$ m. These more sharply-peaked distributions are presumably the result of higher order interactions (which were excluded from the perturbation theory). Such higher order interactions are also responsible for widening the cluster at the incident frequency, ω. The two central lines in Fig. 10 (29σ, 30σ) represent essentially the input from the outer boundary. There is an outer doublet 28σ, 31σ presumably of third order, and an even weaker doublet 27σ, 32σ presumably of fifth order. Similar multiplet broadening is found at the other frequencies, including "zero" frequency. The figure shows an empirical construct in agreement with second order theory which would assign an energy factor $\omega^2 a^2$ for each harmonic increment, and a factor a^2 for each harmonic decrement. With the incident energy of order a^2, we have, for example, the following cubic interactions:

$$\omega + \omega + \omega \text{ of order } a^2 \cdot \omega^2 a^2 \cdot \omega^2 a^2 = \omega^4 a^6$$

$$\omega + \omega - \omega \text{ of order } a^2 \cdot \omega^2 a^2 \cdot a^2 = \omega^2 a^6$$

Apparently many-line interactions lead to multiplet broadening of the central cluster, in the ratio

$$1, \quad \omega^2 a^4, \quad (\omega^2 a^4)^2, \ldots$$

for the energy in successive pairs.

(b) *Frictional Effects*

Friction causes strong multiplet broadening. Frictional effects are of order a^2 in the odd harmonics, and we obtain

Frequency	*Singlet*	*Equivalent multiplet*
$\sim\omega$	$a^2 \cos \omega t$	$\frac{1}{2}a^2 [\cos 28.5\,\sigma t + 2 \cos 29.5\,\sigma t + \cos 30.5\,\sigma t]$
$\sim 3\omega$	$a^2 \cos 3\omega t$	$\frac{1}{2}a^2 [\cos 87.5\,\sigma t + 2 \cos 88.5\,\sigma t + \cos 89.5\,\sigma t]$

Since the interference pattern is precisely repeated each fortnight, the fractional harmonics need to be apportioned among integral harmonics according to

$$\cos (m + \tfrac{1}{2})\sigma t = \pm \frac{2}{\pi} \sum_n \frac{m + \frac{1}{2}}{(m + \frac{1}{2})^2 - n^2} \cos n\sigma t$$

$$\approx \pm \frac{1}{\pi} \sum_n \frac{1}{m + \frac{1}{2} - n} \cos n\sigma t, \quad -\pi \leqslant \sigma t \leqslant \pi,$$

$$= \frac{2}{\pi} [\ldots - \tfrac{1}{3} \cos (m-1)\sigma t + \tfrac{1}{1} \cos m\sigma t$$

$$+ \tfrac{1}{1} \cos (m+1)\sigma t - \tfrac{1}{3} \cos (m+2)\sigma t - \ldots]$$

where $\pm$ refers to $m + n$ even/odd. Thus

$$\cos 28.5\sigma t + 2 \cos 29.5\sigma t + \cos 30\sigma t$$

$$= \ldots (\tfrac{1}{5} - \tfrac{2}{7} + \tfrac{1}{9}) \cos 26\sigma t + (-\tfrac{1}{3} + \tfrac{2}{5} - \tfrac{1}{7}) \cos 27\sigma t$$

$$+ \tfrac{8}{15} \cos 28\sigma t + \tfrac{8}{3} \cos 29\sigma t + \tfrac{8}{3} \cos 30\sigma t + \ldots$$

so that the odd-harmonic triplet with energies $a^4(\frac{1}{4}, 1, \frac{1}{4})$ transforms into the multiplet

$$\left(\frac{8}{3\pi}\right)^2 a^4 [\ldots, 0.00009, 0.00081, 0.040, 1, 1, 0.040, 0.00081, 0.00009, \ldots]$$

as compared to the 3ω mutiplets computed for $\tilde{a} = 5$ cm.:

$$\tilde{k}^2 = 0.001\text{: } 0.368\ a^4 [\ldots, 0.00017, 0.00096, 0.041, 1, 0.98, 0.039, 0.00076, 0.00010, \ldots]$$

$$\tilde{k}^2 = 0.003\text{: } 0.265\ a^4 [\ldots, 0.00023, 0.00137, 0.030, 1, 0.99, 0.030, 0.00110, 0.00012, \ldots]$$

Higher friction spreads an increasing energy into side bands, but the computed energy is less than perturbation theory predicts, particularly for high friction.

(c) *Moon–Sun interaction*

Take first the simplest case of a symmetrical incident doublet

$$\tfrac{1}{2}\sqrt{2}a[\cos 29\sigma t + \cos 30\sigma t] = A(t) \cos 29.5\sigma t,$$

$$A = \sqrt{2}a \cos \tfrac{1}{2}\sigma t$$

According to (4.4), the reflected wave at the outer boundary is given by (ignoring a phase shift of 2ω and setting $\mu = (32/9\pi)k^2\,\phi_1(\omega)$)

$$(A-\mu A^2)\cos 29.5\sigma t = A\cos 29.5\sigma t - \mu a^2 \times (1+\cos\sigma t)\cos 29.5\sigma t = A\cos 29.5\sigma t$$

$$-\tfrac{1}{2}\mu a^2(\cos 28.5\sigma t + 2\cos 29.5\sigma t + \cos 30.5\sigma t) = \frac{\sqrt{2}}{2}a[\cos 29\sigma t + \cos 30\sigma t]$$

$$-\tfrac{1}{2}\mu a^2\frac{2}{\pi}\tfrac{8}{3}[\ldots\cos 29\sigma t + \cos 30\sigma t\ldots] = \frac{\sqrt{2}}{2}a\left[1-\frac{8\sqrt{2}}{3\pi}\mu a^2\right] \times [\ldots\cos 29\sigma t + \cos 30\sigma t + \ldots]$$

The energy dissipated at *each* of the incident doublet frequencies is proportional to

$$a_{\text{inc}}^2 - a_{\text{refl}}^2 \approx \frac{8\sqrt{2}}{3\pi}\mu a^3$$

or $(16\sqrt{2}/3\pi)\,\mu\,a^3$ altogether. For the equivalent singlet, the corresponding loss is

$$a^2 - (a-\mu a^2)^2 = 2\,\mu\,a^3.$$

Doublet dissipation is $8\sqrt{2}/3\pi = 1.18$ that of the equivalent singlet.

In fact the solar to lunar ratio $\varrho = a'/a = 0.46$, and to allow for this approximately we may try equation (6.1) subject to $\varrho = a'/a < 1$. We find, to order ε,

phase modulation, spring:

if $\sigma t = \varepsilon$, $A = a + a'$, $\theta = \varrho\varepsilon$

phase modulation, neap:

if $\sigma t = \pi + \varepsilon$, $A = a - a'$, $\theta = -\varrho\varepsilon$

ampl. modulation, between:

if $\sigma t = \pm\pi/2 - \varepsilon$, $A = a + a'\varepsilon$, $\theta = \pm\varrho$

The reflected wave is

$$A(1-\mu A)\cos(\omega t+\theta) = (1-\mu A)(a\cos\omega t + a'\cos\omega' t)$$

$$= a[1-\mu a(1+\tfrac{1}{4}\varrho^2)]\cos\omega t - a'[1-\tfrac{3}{2}\mu a]\cos\omega' t$$

The lunar and solar dissipations are proportional to (incident amplitude)^2—(reflected amplitude)^2. For the case of Moon *only*, or Sun *only*, these quantities and their ratio are

$$2\,\mu\,a^3 \text{ and } 2\,\mu\,a'^3, \text{ Moon/Sun} = \varrho^{-3} = 10.2$$

respectively, whereas in the presence of both tide-producing bodies we find

$$2\,\mu\,a(a^2+\tfrac{1}{4}a'^2) \text{ and } 3\,\mu\,a\,a'^2 \text{ Moon/Sun} = \tfrac{3}{2}(\varrho^{-2}+\tfrac{1}{4}) = 3.30.$$

With "non-linear amplification"

$$1+\tfrac{1}{4}\varrho^2 = 1.05, \quad \tfrac{3}{2}\varrho^{-1} = 3.25$$

for Moon or Sun, respectively. The ratio 3.3 agrees substantially with the ratio of lunar to solar torques taken by Jeffreys (1952). The total dissipation

$$2\,\mu\,a^3 + 3.5\,\mu\,a\,a'^2 + \ldots$$

is associated with an increase in the length of day, and a progressive increase in the radius of the Moon's orbit about the Earth. Lunar and Solar orbits are significantly coupled in the shallow seas. Since μ is proportional to $\phi_1(\omega)$, this leads to the interesting speculation that the dissipation may vary with the angular velocity ω of the Earth relative to the Moon. For $\omega <$, ≈ 1 we find $\phi_1 \sim \omega^2$, ω, respectively. We need to look into the *variation* of the torque L as a result of the slowing down of the Earth, and compare this effect to that arising from the variable distance to the Moon.

(d) *Incident equilibrium tide*

We now go from the doublet input to the multiplet input of an equilibrium tide at 30° N, directly generated from the known orbital constants of Moon and Sun (Munk & Cartwright, 1966); it consists of the potentials P_2^0, P_2^1, P_2^2 (but not P_3^3). This artificial series $\zeta_{\text{inc}}(t)$ served as an input function for the standard shelf, and the associated tide at the sea wall $\zeta(t)$ was computed in the usual manner. In addition, we derived $\xi(t)$, as the best possible (in the least square sense) linear prediction of

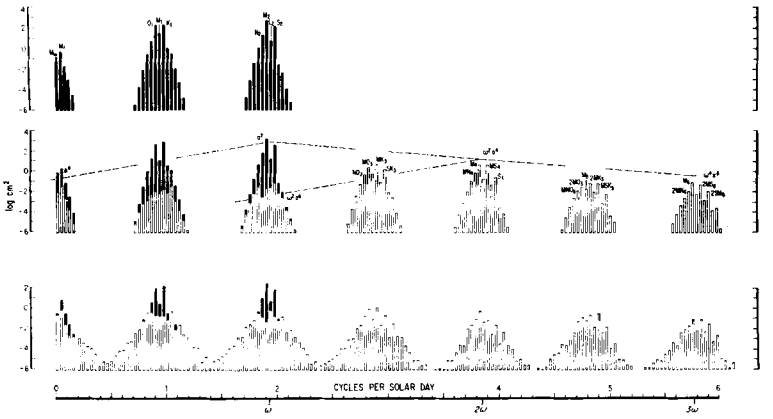

Fig. 11. The spectrum of the incident equilibrium tide (*top*) and the computed tide at the sea wall for the cases of no friction and friction ($\tilde{k}^2 = 0, 0.003$), respectively. The unfilled portions of the columns designate the energy of the non-linear component of the sea wall tide. Some "Darwin-Zetler" symbols are given. The left scale refers to energy per column, with band width 1 cycle-per-month. The ω-scale (in cycles per half lunar day) is included for comparison with previous displays.

$\zeta(t)$, based on $\zeta_{\text{inc}}(t)$. The residual $\zeta_{\text{res}}(t) = \zeta(t) - \tilde{\zeta}(t)$ is presumably the result of non-linear processes.

The three series ζ_{inc}, ζ, ζ_{res} were generated for a length of 3 months, and then multiplied by a function which gently fades to zero at start and finish. In this manner the side bands of frequencies that are not integral harmonics of the record length are substantially reduced. The power of each harmonic of the faded 3 month records was computed and three adjoining harmonics combined to yield estimates of power within cycle-per-month bands. Within each series the bands were precisely centered at the frequencies of the principal components. All these precautions are required to avoid truncation side bands which would otherwise mask the non-linear effects.

Fig. 11 shows the resulting spectra of incident, total and residual tides. We can visualize the previous analysis of the doublet as arising from the M_2, S_2-interaction. As new features we have the "diurnal inequality" associated with the incident diurnal energy (frequency $\frac{1}{2}\,\omega$), plus, of course the added complexity of the ω-incidence and some low frequency input.

The total incident energy in the ω-multiplet is 800 cm², hence $a^2 = 3.12 \times 10^{-4}$. The dashed curves are drawn as in Fig. 10, but they give a poor indication of non-linear effects. There are no simple guide lines for the frictional case. The principal conclusion is that the resulting spectra are of such complexity as to discourage predictions of highly non-linear tides in the frequency domain.

There remains the question of whether the enhancement of actual, observed spectra in the vicinity of strong lines can be attributed to the many-line problem (and hence be predictable), or whether it represents a line–noise interaction. From the work of Zetler (1967) it appears that for species 3, 4, 5, ... the multiplet energy can account for most of the observed tidal energy of shallow water ports. For the "O frequency" species multiplet energy is relatively unimportant as compared to the meteorologically induced continuum which obscures all but the strongest lines. For the principal energy at 1 and 2 cycles-per-day the many–line interaction within the incident multiplet, as considered here, is certainly a factor, especially at the outer skirts of the species, but otherwise the enhanced energy found between the lines must be the result of line–noise interactions.

REFERENCES

Bowden, K. F. & Fairbairn, L. A. 1952. A determination of the frictional forces in a tidal current. *Proc. Roy. Soc. A 214*, 371–392.

Jeffreys, H. 1958. Review. *J. Fluid. Mech. 4*, 335.

Keller, J. B. & Keller, H. B. 1964. Water wave run-up on a beach. *Research Report*, Service Bureau Corporation, New York. 32 pp.

Lamb, H. 1932. *Hydrodynamics*. Dover Publications, New York. 738 pp.

Longuet-Higgins, M. S. & Stewart, R. W. 1964. Radiation stress in water waves; a physical discussion, with applications. *Deep Sea Res. 11*, 529–562.

Munk, W. H. & Cartwright, D. E. 1966. Tidal spectroscopy and prediction. *Phil. Trans.* A. *259*, 533–581.

Rossiter, J. R. & Lennon, G. W. 1965. Computation of tidal conditions: the Thames estuary by the initial value method. *Min. Proc. Instn Civ. Engrs 31*, 25–56.

Stoker, J. J. 1957. *Water waves*. Interscience, New York. 567 pp.

Taylor, G. I. 1919. Tidal friction in the Irish Sea. *Phil. Trans. Roy. Soc.* A *220*, 1–33.

Unoki, S. & Isozaki, I. 1965. Mean sea level in bays. *Oceanogr. Mag. 17*, 11–35.

Ursell, F. 1953. The long-wave paradox in the theory of gravity waves. *Proc. Camb. Phil. Soc. 49*, 685–694.

Zetler, B. D. & Cummings, R. A. 1967. A harmonic method for predicting shallow-water tides. *J. Marine Res. 25*, 103–114.

Notation

$\tilde{x}, x$	dimensional, and dimensionless distance, positive shoreward	L	width of shelf
$\tilde{t}, t$	time	$f_0, f_1, f_2, \ldots$	harmonics of tidal elevation, frequencies 0, ω, 2ω, ...
$\tilde{a}, a$	incident wave amplitude	u_1, u_2	hamonics of flow velocity, frequencies ω, 2ω, ...
$\tilde{\zeta}, \zeta$	tidal elevation	$\alpha_1 \alpha_2, \ldots$	harmonics of reflected wave elevation
H	undisturbed water depth	$\tilde{k}^2, k^2$	friction parameter
$h = H + \zeta$	total water depth	$\zeta = -\omega(x-1)$	dimensionless distance, positive seaward
$\tilde{u}, u$	flow velocity	$\zeta, \tilde{\zeta}$	observed and predicted tides
$\tilde{c}, c$	wave velocity		
$\tilde{\omega}, \omega$	frequency		
$\tilde{\varkappa}, \varkappa$	wave number		

ПРИЛИВЫ В МЕЛКОЙ ВОДЕ: СПЕКТРОСКОПИЯ

Анализируются нелинейные искажения длинных волн (приливов) на мелководье. Эффекты конечности амплитуды, наклона дна, трения и многокомпонентные взаимодействия изучаются отдельно и в комбинации путем использования как метода возмущений, так и численного решения полных нелинейных уравнений. Искажения, вызываемые каждым источником нелинейности, представлены в пространствах времени и частот. Обсуждаются некоторые следствия полученных результатов для предсказания приливов в локальных и глобальных масштабах океана.